LA-7477-MS
Informal Report

C3

Injection of Laser Fusion Pellets

Part I

Accuracy Required, Acceleration, and Residual Gas Deflections

LOS ALAMOS SCIENTIFIC LABORATORY
Post Office Box 1663 Los Alamos, New Mexico 87545

UNITED STATES
DEPARTMENT OF ENERGY
CONTRACT W-7405-ENG. 36

LA-7477-MS
Informal Report
UC-21
Issued: September 1978

Injection of Laser Fusion Pellets

Part I

Accuracy Required, Acceleration, and Residual Gas Deflections

Joseph J. Devaney

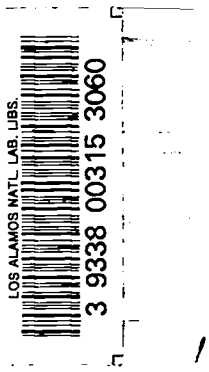

INJECTION OF LASER FUSION PELLETS
PART I
ACCURACY REQUIRED, ACCELERATION, AND RESIDUAL GAS DEFLECTIONS

by

Joseph J. Devaney

ABSTRACT

In order to position a pellet within a laser fusion power plant reactor chamber accurately enough so that sufficient light will illuminate the desired portions of the pellet, one must know for the pellet: the positional accuracy required, the accelerations (structurally) permissible, and the perturbing effect on the pellet trajectory of residual gas motion. This report purports to answer these questions by a number of representative calculations. It is found that neither positional accuracies, typical pellet structure, available pellet accelerations, nor the highest expected chamber gas densities (nor the lowest) permitted by efficient laser beam transport, are any restraint upon pellet insertion save at high repetition rates (> 10/s) when the other parameters have latitude for, and require (at least some) optimization.

I. INTRODUCTION

In order to position a pellet within a laser fusion power plant reactor chamber accurately enough so that sufficient light will illuminate the desired portions of the pellet, one must know for the pellet: the positional accuracy required, the accelerations (structurally) permissible, and the perturbing effect on the pellet trajectory of residual gas motion. This report purports to answer these questions by a number of representative calculations. In general we find that pellets can withstand high accelerations and the perturbing effects of debris is negligible.

Section II estimates the pellet position accuracies needed. Section III gives possible accelerations and notes a typical structural acceleration limit. Section IV gives residual gas motion of the pellet debris expanding into vacuum. Section V gives the residual gas motion of the pellet debris expanding into and shocking a background gas. Section VI gives the conclusions that in the range of parameters typical at this writing, pellet deflections and accelerations are acceptable. Our reference pellet[1] for this study has a total mass of 0.3 g and an outer radius of 0.309 cm.

Throughout this report we sometimes use crude scalings or assumptions, the justification of which lies in our intent to calculate a rough upper bound to the effects described.

The chamber gases considered are argon and lithium at particle densities ranging from vacuum to $10^{17}/cm^3$. We fix the chamber ambient temperature at 500° C. Our bounds are not invalidated by conceivable chamber temperature variations.

II. PELLET POSITION ACCURACY REQUIRED

Calculations of the beam position accuracy for the Los Alamos 100-TW Antares laser are based on a wavefront budget of 0.068 λ rms. J. L. Monroe[2] finds that a pointing error of 60 μm (4 s of arc) loses only 2% energy (82% to 80%) out of a 400 μm circle, and for an error of 120 μm (8 s of arc) loses but 4% (82% to 78%) out of a 400 μm circle. For a 1000-μm or 1-mm circle one might then expect that pellet positioning would have to be within the order of 300 μm. Of course the pellet position is relative to the laser beam foci (except for gross displacements), and if pellet positioning and laser firing is not determined by the laser optical trains, then the pellet displacement permissible

error figure of 300 μm must be apportioned among the pellet location error and the laser pointing errors. In addition, if particular parts of a pellet must be illuminated, the above displacement figures also apply for pellet angular errors, θ (in the form $R\theta$, R being the outer radius), such that $\theta < \sqrt{2}$ radians. Detailed designs are not yet in hand upon which angular analysis can be based. Generally the least restrictive pellets in all displacement error dimensions are outer surface illuminated, symmetric pellets in which the whole area of the pellet is to be illuminated. In that case orientation is not required, and the largest translational displacement error is permitted.

III. PELLET ACCELERATIONS PERMISSIBLE

We give a number of representative calculations of the accelerations permissible for various structural members of a typical pellet. For orientation we first present a number of conceivable accelerations and some expected decelerations. Consider for example a 100-cm-long pneumatic pellet gun powered by hydrogen at the chamber ambient temperature of 500°C. Neglecting viscosity and friction but correcting for rarefaction, (see Appendix), we get the results given in Table I.

The amount of hydrogen used to inject the pellet is equal to the tube volume at the time of gas shut off, t_s. This time is less than the time of acceleration down the tube because the rarefaction wave signalling closure of the hydrogen supply travels at finite speed, to wit the sound speed c = 2.11 x 10^5 cm/s in 500°C H_2 at 1 atm. We here ignore the slight change in c caused by the pellet velocity rarefaction of the Appendix. Thus if $t = \sqrt{2s/a}$ is the time of acceleration, s being the length and a the (constant) acceleration, then the difference,

$$t - t_s = s/c$$

from which

$$t_s = \sqrt{2s/a} - (s/c) = 0.0136s.$$

The minimum volume of H_2 gas released in the chamber is

$$V = (\pi/2)aR^2t_s^2 = 28 \text{ cm}^3,$$

R = 0.309 cm being the pellet radius. At 1 atm H_2 and a temperature of 500°C this volume contains 2.66 x 10^{20} molecules, which spread out over a cylinder of 250-cm radius by 2400-cm long adds 5.65 x 10^{11} molecules/cm^3. This perturbation is negligible compared to the usual chamber densities considered (10^{13} to 10^{17} particles/cm^3).

To obtain the maximum pellet drag in the chamber, we study argon at a particle density of 10^{17}/cm^3. The drag force at high speeds is

$$F_D = C_D \tfrac{1}{2} \rho v^2 (\pi R^2), \qquad (1)$$

where C_D is the coefficient of drag, ρ the gas density, v the pellet velocity, and R the pellet radius. The coefficient of viscosity, η, is related to the kinematic viscosity, ν, by

$$\nu = \eta/\rho. \qquad (2)$$

The Reynolds number, $\mathcal{R}$, is given as

$$\mathcal{R} = vd/\nu = vd\rho/\eta, \qquad (3)$$

if d is the pellet diameter. At 500°C and 1 atm the viscosity, η, of argon is about 448 micropoises,[3] and that of lithium we estimate lies between that for hydrogen and mercury. We therefore take η of lithium to be 285 micropoises.

The decelerations at various speeds (Table I) are given in Table II. The decelerations in Table II are negligible compared to those of acceleration of the pellet given in Table I. Pellets

TABLE I

PELLET VELOCITIES AND ACCELERATIONS FROM A PNEUMATIC GUN (pellet mass 0.3 g, radius 0.309 cm; gas H_2 at 500°C, gun length 100 cm)

Pressure (atmospheres)	Initial Acceleration (g)	Final Velocity (cm/s)
1	1027.	13,700
0.1	103.	4,489
0.01	10.3	1,419
0.001	1.0	449
(or free fall in vacuum)		

TABLE II

LONGITUDINAL PELLET DRAG

(particle density $10^{17}/cm^3$, radius 0.309 cm, g = 980.7 cm/s^2)

Velocity (cm/s)	Reynold's Number, R	Coefficient of Drag, C_D Ref. 4	Drag Force, F_D (dynes)	Deceleration (g's)
a. Argon				
449	390	0.7	0.14	0.0005
1,419	1,233	0.52	1.04	0.0035
4,489	3,900	0.41	8.2	0.028
13,770	12,000	0.48	90.	0.31
b. Lithium				
449	107	0.98	0.034	0.00012
1,419	337	0.72	0.25	0.0008
4,489	1,066	0.47	1.64	0.0055
13,770	3,270	0.43	14.1	0.048

can stand accelerations typically from 6000 g's upward to well over 100 000 g's so that the highest accelerations or decelerations considered in Tables I and II are not restrictive.

IV. RESIDUAL GAS MOTION - EXPANDING INTO VACUUM

In this section we follow the explosion of a pellet into an evacuated cylinder and calculate the residual gas motion and its effect on the next pellet. For simplicity, in the final stages of the explosion, when it is slowly changing, we take the degree of ionization to be fixed and neglect late recombination. The appropriate ratio of specific heats, γ, for these explosions is 1.4.[5] The spherical explosion is converted by the cylindrical walls (by combination of incident and reflected wave), into a bifurcated plane expansion, that is to a bifolded plane expansion. The slab theory developed by F. J. Dyson[6] therefore applies. His parameter

$$\lambda \equiv (\gamma + 1)/2(\gamma - 1) = 3 \qquad (7)$$

for $\gamma = 1.4$. Whence for large times ($|x| < vt$) the density is

$$\rho = \rho_0 \left[\frac{\Gamma(\lambda - \frac{1}{2})}{\Gamma(\lambda)\Gamma(\frac{1}{2})}\right]\left(\frac{T_1}{t_1}\right)\left[1 - \frac{x^2}{u_1^2 t_1^2}\right]^{\lambda-1}$$

$$= \rho_0 (3/8)(T_1/t_1)\left[1 - (x^2/u_1^2 t_1^2)\right]^2, \qquad (8)$$

where ρ_0 is the initial density of the slab, u_1 is the velocity of the gas fronts, and x the distance from the slab center,

$$u_1 \equiv 2/(\gamma - 1)\, c_0 = \left[2/(\gamma - 1)\right]\sqrt{A\gamma\rho_0^{\gamma-1}}$$

$$u_1 = 5\sqrt{1.4\, A\rho_0^{0.4}}\,. \qquad (9)$$

These formulae are based on an equation of state of the form

$$P = A\rho^{\gamma} = A\rho^{1.4}, \qquad (10)$$

where A is a constant, P the pressure, c_0 the initial speed of sound, t_1 is the time from the start of motion, and T_1 is the time it takes for the rarefaction waves to meet in the center. T_1 is equal to half the original thickness, H, divided by the speed of sound, c_0,

$$T_1 = H/c_0. \qquad (11)$$

The velocity v_1 at position x and time t_1 is simply

$$v_1 = x/t_1. \qquad (12)$$

We return now to the early spherical expansion into vacuum before the explosion reaches the cylindrical walls. By generalizing Devaney[7] to $\gamma = 1.4$, his equation of the density in a spherical explosion of total mass M is

$$\rho = (35\, M/12\, R^3)\left[1 - (r^2/R^2)\right]^2, \qquad (13)$$

and the total (particle) energy is

$$E = 4\, MR^2/27t^2 = 4\, M\bar{u}^2/27, \qquad (14)$$

where the maximum velocity, u, is

$$\bar{u} = R/t = \left[2/(\gamma - 1)\right] c_0, \qquad (15)$$

and the velocity within the expanding spherical gas is

$$u = r/t. \qquad (16)$$

Having now the velocities and densities of both a planar and a spherical explosion, we must transfer from the latter to the former. That part of the spherical explosion that is directed along the axis suffers no appreciable change. That part of the explosion that reflects off the cylindrical walls forms, by combining the original with the reflected gas, a combined gas flow similar to a Mach stem in blast wave theory, and contributes to the down axis flow, a gas flow of the same order as (or perhaps larger than) the on-axis flow itself. So it is reasonable to take the axis flow as suitable for matching spherical to plane flow. Indeed, comparison of formula (13) for spherical flow and formula (8) for plane flow show the same shape and nearly the same analytic dependence on the variables. We match at equal volumes and equal on-axis gas fronts, including frontal on-axis velocities. Let the cylinder radius be R_c, the spherical gas outer radius R, and the axial distance, x. We require at matching time that the spherical volume equal the cylindrical volume, or

$$4\pi R^3/3 = \pi R_c^2 \cdot 2x \text{ at match.} \qquad (17)$$

Equal location of the on-axis gas fronts imply

$$x = R \text{ at match,} \qquad (18)$$

so that, using $R_c = 250$ cm,

$$R_m = \sqrt{\frac{3}{2}} \cdot 250 = 306.2 \text{ cm at match.} \qquad (19)$$

$x_m = R_m$ are the matching distance parameters of planar and spherical flows respectively. Using Eq. (18) and comparing Eqs. (13) and (8) we find

$$\rho_0(3/8)(T_1/t_{1m}) = 35\ M/12\pi R_m^3 \text{ at match,} \qquad (20)$$

and

$$u_1 t_{1m} = R_m \text{ at match.} \qquad (21)$$

So determining the parameters of the plane flow from those of the spherical explosion.

Because our expansion is predicated on a fixed degree of ionization together with neglect of radiative effects, it is accurate for later times only, so we do not start our spherical expansion by substituting the initial energy into Eq. (14). Rather we utilize detailed machine calculations for initial expansion and use our theory to continue the expansion only in its later stages. At 5.1×10^{-8} s the outer radius of our reference pellet has reached 2.67 cm with an average temperature of 86 eV for the outer parts containing 2/3 the pellet mass. We scale this pellet to larger radii and times using a lower yield pellet of the same type that was calculated to later times. We thus find our reference pellet at 3.15 μs after start of laser light deposition to have an outer radius, R = 189 cm, and an average outer part temperature of 2.3 eV. At 51 ns we have in the pellet a total kinetic and internal energy of 24.4 MJ, the remainder of the explosive energy having been carried away by neutron and x-ray radiation. Scaling to 3.15 μs the energy available for expansion has dropped to 22.7 MJ, the rest also having been lost to radiation in the interim. We take further radiation losses to be negligible and so substitute $E = 22.71 \times 10^{13}$ ergs plus M = 0.3 g in Eq. (14) to find

$$\bar{u} = 7.13 \times 10^7 \text{ cm/s} = u_1, \qquad (22)$$

where we will take the gas front velocities of the spherical and planar expansions to be the same at match time. At R = 189 cm, Eq. (22) gives a time t = 2.65 μs. This time, t, is characteristic of an explosion of 0.3 g and 22.7 MJ whereas the time 3.15 μs includes compression, and burn times as well as an initially faster expansion followed by very considerable radiative energy loss. Using Eqs. (22) and (19), the effective spherical match time, t_m, is 4.30 μs. Using Eq. (20),

$$\rho_0(3/8)(T_1/t_{1m}) = 9.76 \times 10^{-9} \text{ g/cm}. \qquad (23)$$

Equations (20) and (22) yield

$$t_{1m} = 4.30 \times 10^{-6} \text{ s.} \qquad (24)$$

Thus, using Eqs. (23) and (24), Eq. (8) becomes

$$\rho = (4.19 \times 10^{-14}/t) \cdot$$

$$\left[1 - (x^2/(7.13 \times 10^7)^2 t^2)\right]^2 \text{ g/cm}^3, \qquad (25)$$

where we have used the fact that the spherical and planar times are identical, $t = t_1$.

Equations (12) and (25) give us the parameters needed to estimate the effect on the next inserted pellet

$$v_1 = x/t. \qquad (12)$$

It is hard to imagine the explosion symmetry from a preceding pellet being as much as 5 mm off from the position of the next pellet, but we chose that number as a conservative estimate. At a repetition rate of 10/s the density and velocity are

$$\rho_{0.1} = 4.19 \times 10^{-13} \text{ g/cm}^3,$$

$$v_{0.1} = 5 \text{ cm/s}, \qquad (26)$$

and at a repetition rate of 1/s the density and velocity are

$$\rho_1 = 4.19 \times 10^{-14} \text{ g/cm}^3,$$

$$v_1 = 0.5 \text{ cm/s}. \qquad (27)$$

The transverse drag forces can be obtained using Eq. (1) for a radius 0.309 cm to get $F_D = 1.57 \times 10^{-12} C_D$ dynes at 10/s and $1.57 \times 10^{-15} C_D$ dynes at a 1/s repetition rate. These are utterly negligible forces for any drag coefficient. Actually the vacuums represented by these densities are more tenuous than typical or needed in vacuum reaction chamber. The low results of Eqs. (26) and (27) simply indicate that the chamber has returned to quiescence by the time the next pellet is inserted so that it is not deflected by remaining debris motion.

A calculation for $\gamma = 1.67$ (monatomic) and for a higher, 10/s repetition rate yields a larger effect:

$$\rho_1 = 7.7 \times 10^{-8} \text{ g/cm}^3 \text{ and } v_1 = 5 \text{ cm/s}, \qquad (28)$$

which at 5 mm successive pellet stagger and $C_D = 1.26$ leads to a deflection of 0.16 μm, still a negligible displacement.

Conclusion: In a vacuum chamber, and for repetition rates near or less than 10/s, pellet injection is not deflected by residual gas motion.

V. RESIDUAL GAS MOTION - BACKGROUND GAS, BLAST-WAVE, ACOUSTIC RINGING

In the presence of a background gas in the chamber, the microexplosion sets up first a spherical blast wave which the cylindrical walls convert into two (roughly) plane waves that alternately reflect from the ends and then from each other at the center repeatedly, being damped by pressure and matter loss at the ends (wall and gas viscosity losses are negligible and their omission conservative), eventually exciting the acoustic modes of the chamber of which the fundamental will dominate in time, but we will actually find it having dominant excitation right after the first end reflection. Our method of calculation is first to employ the brilliant self-similar analysis of Sedov[8] describing the expansion of a spherical blast wave which we then reflect off a cylinder to form, with the resulting Mach stems, a plane blast wave, the parameters of which we match along the axis with the original spherical blast wave. We propagate the plane blast wave to the ends. There we cannot use simple self-similar reflection theory because the densities, temperatures, and pressures in the chamber are now far from constant. With the help of H. Ruppel, the code YAQUI was used to reflect the blast wave from the end and into its own tail, to eventually form a nearly perfect fundamental acoustic mode of the chamber. Although the amplitude of the wave at this early time is large and therefore quite evidently nonlinear, we argue that early application of acoustic theory is conservative, i.e., acoustic wave losses are less than those for nonlinear waves, and we will follow the dynamics of the damped acoustic wave until insertion of the next pellet.

For maximum effect we choose the highest density background gas and so consider argon at an initial particle density of $.10^{17} \text{cm}^3$ and a temperature of 773K leading to densities of 6.63×10^{-6} g/cm^3 and pressures of 10 672 d/cm^2 or 8 torr. To mock up the extra degrees of freedom of ionization and recombination we retain $\gamma = 1.4$. The theory easily handles other γ's. Because the blast wave begins early, caused by the rapid pellet expansion, we conservatively cut off radiative losses also early and start the spherical blast wave in

the argon with 24.4 MJ energy at 51 ns. It should be understood that the original explosive energy is considerably larger than 24 MJ. Following now Sedov's notation we relabel the total energy, E_0 = 24.4 MJ, and reserve E for an energy parameter, the two being related by

$$E_0 = \alpha E, \tag{29}$$

where, from Sedov's Fig. 75, for $\gamma = 1.4$: $\alpha = 0.85$ for spherical blast waves and $\alpha = 1.105$ for plane blast waves.

Sedov's formulae (11.4) and (11.6) give the shock position, r_2, and speed, v_2, as a function of time, E, and the initial density, ρ_1. For the special case,

$$E = 2.87 \times 10^{14} \text{ ergs}, \tag{30}$$

$$r_2 = (E/\rho_1)^{1/5} t^{2/5}, \tag{31}$$

$$v_2 = (2/5)(E/\rho_1)^{1/5} t^{-3/5}$$

$$= (2/5)(E/\rho_1 r_2^3)^{1/2}. \tag{32}$$

For the plane case,

$$E = 2.21 \times 10^{14} \text{ ergs}, \tag{33}$$

if started as a plane shock, but see below, Eq. (44) for the value we use.

$$r_2 = (E/\rho_1)^{1/3} t^{2/3}, \tag{34}$$

$$v_2 = (2/3)(E/\rho_1)^{1/3} t^{-1/3}$$

$$= (2/3)(E/\rho_1 r_2)^{1/2}. \tag{35}$$

Solving Eq. (31) for t,

$$t = r_2^{5/2}(E/\rho_1)^{-1/2}, \tag{36}$$

we substitute the spherical to plane match radius, 306.2 cm, Eq. (19) to find

$$t_m = 2.494\ \mu s. \tag{37}$$

At this time we convert the spherical blast wave to a plane wave of the same strength along the axis. That is a rigorous match at the axis and perhaps a somewhat inferior match elsewhere because the Mach stems formed by the incident and reflected waves from a rigid cylinder wall can be of greater strength than the initial wave alone. However, in the case of magnetic fields, the off axis waves are less strong because the shock does work in compressing the magnetic field. However in all cases it is a reasonable approximation to take the axial spherical shock strength at t_m to be the plane shock strength. As before, we match when the spherical and cylindrical volumes are equal, Eqs. (17) and (18), to get r_{2m} = 306.2 cm, Eq. (19). Sedov gives for the shock pressure,

$$P_2 = \left\{8\rho_1/[(\nu + 2)^2(\gamma + 1)]\right\} \cdot$$

$$(E/\rho_1)^{2/(2+\nu)}\ t^{-2\nu/(\nu+2)}$$

$$= 8E/\left[(\nu + 2)^2(\gamma + 1)r_2^{\nu}\right], \tag{38}$$

where $\nu = 1$ for plane flow, $\nu = 2$ for cylindrical, and $\nu = 3$ for spherical flow. Thus for our parameters, at match,

$$P_{2m} = 1.333 \text{ d/cm}^2. \tag{39}$$

We match pressures and distances and determine a new time, t', and energy parameter E'. Primes now refer to planar motion. We will show, as a consequence, that the shock velocities are identical at match point.

For $\nu = 3$, spherical, Eq. (38) gives

$$P_2 = 8E/\left[25(\gamma + 1)r_2^3\right], \tag{40}$$

and for plane, $\nu = 1$,

$$P_2 = 8E'/\left[9(\gamma + 1)r_2\right], \tag{41}$$

equation p_2 and r_2 at match leads to the relation

$$E' = (9/25\ r_{2m}^2)E. \tag{42}$$

Substituting E' for E in Eq. (35) we get the plane shock velocity, v_2',

$$v_2' = (2/5)(E/\rho_1 r_{2m}^3)^{1/2} = v_2, \tag{43}$$

which is precisely the spherical shock velocity, v_2, of Eq. (32), proving that matching pressure and distance ensures a velocity match, as alleged.

At match then Formula (42) yields

$$E' = 1.102 \times 10^9 \text{ ergs.} \quad (44)$$

Formula (41) becomes

$$P_2 = 4.08 \times 10^8/r_2, \text{ d/cm}^2, \quad (45)$$

and (35) becomes

$$v_2 = 8.59 \times 10^6 \, r_2^{-1/2} \text{ cm/s.} \quad (46)$$

From which the fluid velocity is

$$u_2 = 2v_2/(\gamma + 1), \quad (47)$$

or for $\gamma = 1.4$

$$u_2 = 7.16 \times 10^6 \, r_2^{-1/2} \text{ cm/s.} \quad (48)$$

The plane shock time, t', is given by Formula (34) divided by (35),

$$t' = 2r_2/3v_2 = 7.758 \times 10^{-8} \, r_2^{3/2} \text{ s.} \quad (49)$$

This time is only applicable between match and cylinder ends. It took 5.1×10^{-8} s to compress (by laser light) the pellet, burn the DT, and expand to 2.67 cm where we picked up a (Sedov) spherical blast wave. The spherical blast wave time at 2.67 cm is given by Eq. (36) and is 1.771×10^{-9} s. Thus the real time to match point is 2.495 μs and the real time elapsed, τ, beginning with lasers on pellet to plane expansion at r_2 is

$$\tau = t' - 1.662 \times 10^{-4}$$

$$\tau = 7.758 \times 10^{-8} \, r_2^{3/2} - 1.662 \times 10^{-4} \text{ s,} \quad (50)$$

so that for $r_2 = 1200$ cm, $\tau = 3.059 \times 10^{-3}$ s. The density increase in a strong shock is given by

$$\rho_2 = \left[(\gamma + 1)/(\gamma - 1)\right] \rho_1$$

$$= 6\rho_1 = 3.98(-5) \text{ g/cm}^3. \quad (51)$$

The temperature (if we can now switch to a simple un-ionized perfect gas law) is

$$T_2 = p_2 A/\rho_2 R. \quad (52)$$

We approximate the actual end wall configuration by end plates (with exhaust holes) at 1200 cm from the center. At that position, just before the shock strikes the end we have the peak shock parameters:

Pressure

$$P_2 = 3.40 \times 10^5 \text{ d/cm}^2 \quad \text{Eq. (45)} \quad (53)$$

Shock velocity

$$v_2 = 2.48 \times 10^5 \text{ cm/s} \quad \text{Eq. (46)} \quad (54)$$

Fluid velocity

$$u_2 = 2.07 \times 10^5 \text{ cm/s} \quad \text{Eq. (48)} \quad (55)$$

Real time

$$\tau = 3.059 \times 10^{-3} \text{ s} \quad \text{Eq. (50)} \quad (56)$$

Density

$$\rho_2 = 3.98 \times 10^{-5} \text{ g/cm}^3 \quad \text{Eq. (51)} \quad (57)$$

Temperature

$$T_2 = 4{,}104\text{K} \quad \text{Eq. (52)} \quad (58)$$

Using Sedov's tables, p. 222, one can easily determine from these values the values of particle velocity, density, and pressure between r = 1200 and 0 cm. The velocity distribution is nearly proportional to the distance from the origin, being very slightly peaked toward r_2. On the other hand the temperature rises sharply as r decreases and so must be considered unphysical for small enough distances from the center (radiation losses, if included, would prevent such extreme temperatures). Both the pressure and the density are strongly peaked forward, the former dropping from its maximum value at $r_2 = 1200$ cm to an asymtotic 40% of maximum for $r \leq 600$ cm. The density drops to zero with decreasing r; it has dropped to half value at r = 1080 cm and is down to 0.06 of maximum at 600 cm.

With such sharp density, pressure, and temperature variations, simple shock reflection into constant density residual gas is wholly inappropriate. Accordingly it was necessary to resort to a machine calculation to reflect the shock from the end wall and to propagate the reflected wave toward the center. Through the kindness of H. Ruppel the problem of first reflection was run using the code YAQUI. Inputs were the above described density and

fluid velocities versus distance plus an equation of state of the form

$$P = (\gamma - 1)\rho I, \qquad (59)$$

I being the internal energy, 2.14×10^{10} ergs/g, which we took from the peak values, Eqs. (53) and (57). Figure 1 shows a typical half cylinder planar result at time $\Delta\tau = 3.3 \times 10^{-3}$ s after reflection. In Fig. 1 we plot the now inward velocity, u, and the pressure p versus distance. Because of collapse of the computing mesh the values of x between 0 and 200 cm are oscillating and are consequently unreliable. The values for this run are slightly higher than warranted by our present input; P being 12% higher in Fig. 1, and u being 6% higher. The shape of the wave is nearly that of the fundamental acoustic wave of the chamber, = 2400 cm. The velocity is nearly symmetric and shows a negative peak for positive x and would show a corresponding positive peak for negative x if plotted. The pressure is dominated by a pressure peak at the ends, but its minimum does not occur at x = 0 as it should for a perfect fundamental wave. In any case not only is the wave already nearly fundamental, but we expect the fundamental mode to dominate eventually because of higher damping of the harmonics. We therefore analyze Fig. 1 (corrected) for the fundamental mode strength by numerical integration. Thus we calcualte the standing wave,

$$u = +(A/\langle\rho\rangle c)\sin(\pi x/L)\sin(\omega t + \phi), \qquad (60)$$

$$P = \langle P\rangle + A\cos(\pi x/L)\cos(\omega t + \phi), \qquad (61)$$

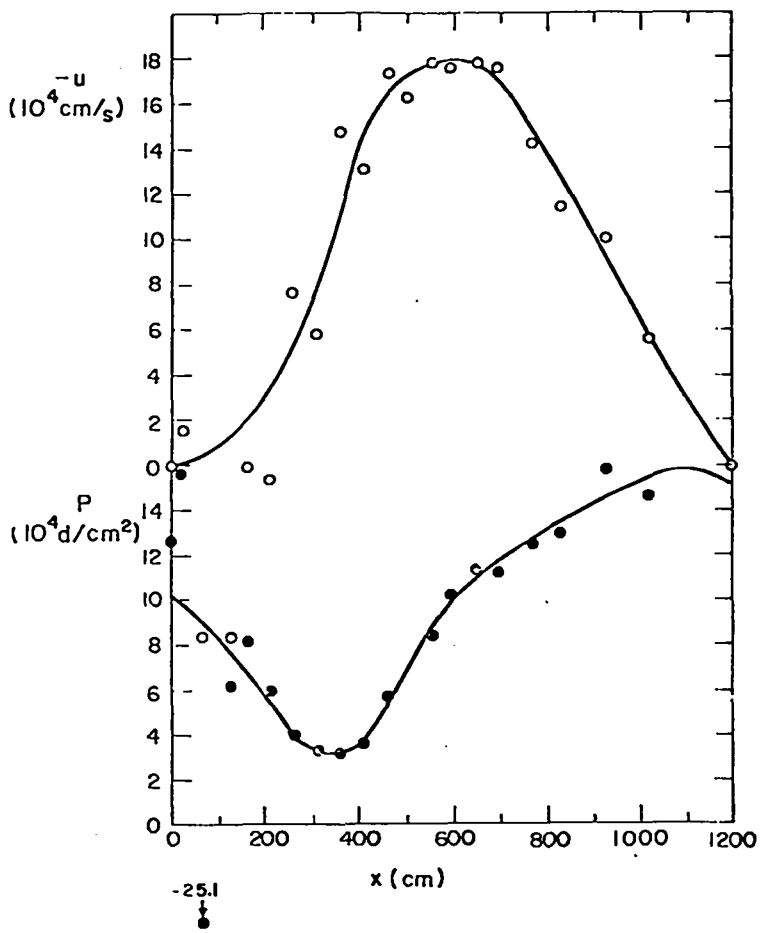

Fig. 1. Velocity and pressure after blast wave reflection (0.0033s) at end with no hole (Calculation III, Cycle 151).

where A is the amplitude, $\langle\rho\rangle$ the mean density, c the speed of sound, L is the half-chamber distance, 1200 cm, ω is the angular frequency, ϕ is the phase.

From the mean internal energy, I = 2.72 x 10^{10} ergs/g, evaluated using Eq. (59) and only from 360 cm to 1200 cm so as to avoid mesh collapse uncertainties, and using the formula

$$c = \sqrt{\gamma I} = \sqrt{1.4\ I}, \qquad (62)$$

we find

$$c = 1.952 \times 10^5 \text{ cm/s}. \qquad (63)$$

The pellet debris only increases the mean density 0.01% over the original argon density of 6.634 x 10^{-6}, thus

$$\langle\rho\rangle = 6.635 \times 10^{-6} \text{ g/cm}^3. \qquad (64)$$

The mean pressure from Fig. 1 (less 12%) is

$$\langle P\rangle = 89{,}900 \text{ d/cm}^2, \qquad (65)$$

and we estimate the peak pressure to be

$$\bar{P} \sim 168{,}000 \text{ d/cm}^2,$$

so that at t = 0, x = L, and using Eq. (61)

$$\bar{P} - \langle P\rangle \equiv \Delta P = 77{,}900 \text{ d/cm}^2 = -A\cos\phi. \qquad (66)$$

From a numerical integration of the velocity curve of Fig. 1 (less 6%) and comparison with integration of Eq. (60) at t = 0, we find

$$(A/\langle\rho\rangle c)\sin\phi = -137{,}600 \text{ cm/s}, \qquad (67)$$

so that using Eqs. (64) and (65)

$$A\sin\phi = -178{,}300. \qquad (68)$$

Solving Eqs. (66) and (68) we get

$$\phi = 1.159 \text{ radians}, \qquad (69)$$

$$\Delta\bar{P} \equiv A = -194{,}600, \qquad (70)$$

so that the maximum velocity is

$$-\bar{u} \equiv (A/\langle\rho\rangle c) = -150{,}200 \text{ cm/s}. \qquad (71)$$

The angular frequency, ω, is determined from

$$\omega = 2\pi f = 2\pi c/\lambda = \pi c/L, \qquad (72)$$

whence using Eq. (63)

$$\omega = 511 \text{ radians/s}, \qquad (73)$$

the period, , and frequency, f, are

$$= 1/f = 2\pi/\omega = 2L/c = 0.01229 \text{ s}, \qquad (74)$$

$$f = \omega/2\pi = c/2L = 81.35 \text{ s}^{-1}. \qquad (75)$$

Thus, Eqs. (60) and (61) become

$$u = -150{,}200 \sin(\pi x/1200) \cdot \sin(511\ t + 1.159), \qquad (76)$$

$$P = 89{,}900 - 194{,}600 \cos(\pi x/1200) \cdot \cos(511\ t + 1.159). \qquad (77)$$

That the amplitude of pressure oscillations exceeds the mean is unphysical and results from premature substitution of the linear (acoustic) theory for the nonlinear theory. Our justification for such early substitution is threefold. First we have not yet included damping which will reduce A, although not usually below $\langle P\rangle$ after only one end bounce for small aperture exhaust ducts. Second, early use of linear theory is conservative, the nonlinear wave damps faster, so we overestimate effects. Third, within our level of approximation, early linear substitution is not unreasonable.

The time t of Eqs. (75) and (76) begins as of Fig. 1. Real time, τ, since the beginning of the laser light pellet interaction is related to this t by Eq. (50) to r_2 = 1200 cm plus time to cycle 151 of Fig. 1).

$$\tau = 6.359 \times 10^{-3} + t \quad \text{s}. \qquad (78)$$

Each time the wave hits the ends a portion of the wave is lost to the exit orifices. Scaling a typical size exhaust duct from a wetted wall design[9] of 4.2 m^3 volume to our 471 m^3 volume we choose each exhaust duct to have a radius of 100 cm. For this orifice we will assume (Case I) that $(100/250)^2$ = .16 of the over-pressure and velocity amplitudes are lost with each reflection. In case the chamber has conically narrowed ends leading to the orifice, or if the orifice is larger than 100 cm, then more is lost per reflection so we also consider a case (II) in which half the over-pressure and velocity amplitudes are lost per reflection. Thus for Case I, Eqs. (76) and (77) become:

$$u = -150{,}200(0.84)^{(0.00899 + t)/.01229} \cdot \sin(\pi x/1200)\sin(511\ t + 1.159)\ ,$$

$$\equiv A_u \sin(\ x/1200)\sin(511\ t + 1.159)\ . \quad (79)$$

$$p = 89{,}900 - 194{,}600(0.84)^{(0.00899 + t)/.01229} \cdot \cos(\pi x/1200)\cos(511\ t + 1.159),$$

$$P \equiv \langle P \rangle - A\cos(\pi x/1200)\cos(511\ t + 1.159). \quad (80)$$

The 0.00899 in the exponent accounts for the first (machine calculated) reflection at the ends less the time to arrive at the configuration of Fig. 1, t = 0 here. We will consider two pellet velocities (Table I), fast (f), 13 770 cm/s, and slow (s), 449 cm/s; and two repetition rates; 1/s (τ = 1 s) and 10/s (τ = 0.1 s). We calculate the maximum pellet deflection at x = 0.5 cm, a rather large departure from symmetry of one explosion to the next, but a highly possible departure for a nonsymmetric chamber. Pellet deflection is caused by change in pressure and by aerodynamic drag; these are 90° out of phase, however. The side, b, of a cube of the same volume as a sphere of radius r is

$$b = (4\pi/3)^{1/3}\ r. \quad (81)$$

From Eq. (80) the pressure change across b is

$$p = +(\pi A/1200)\sin(\pi x/1200) \cdot \cos(511\ t + 1.159)(4\pi/3)^{1/3}\ r, \quad (82)$$

with the force being

$$F_p = \Delta P b^2 = (\pi^2 A/900)r^3 \sin(\pi x/1200) \cos(511\ t + 1.159), \quad (83)$$

and the deflection from the wave pressure being (for small Δx)

$$\Delta_p = (1/2)at^2 = F_p R_c^2/2mv^2. \quad (84)$$

R is the cylinder radius, m the pellet mass, and v the pellet transverse velocity. From aerodynamic drag the force is

$$F_u = C_D(1/2)\rho u^2 \cdot \pi r^2 = (\pi C_D \rho A_u^2/2)r^2 \sin^2(\pi x/1200) \cdot \sin^2(511\ t + 1.159), \quad (85)$$

and the contribution to displacement is

$$x_u = F_u R_c^2/2mv^2. \quad (86)$$

The coefficient of drag is determined from Table II, since the total velocity governs.

Table III gives the maximum possible deflection from the residual gas pressure gradient, $\overline{\Delta x}_p$, and the velocity drag, $\overline{\Delta x}_u$ which are 90° out of phase with each other.

If the symmetry of the chamber is greatly compromised then pellet insertion might occur at equivalent asymmetries of more than 0.5 cm from the central node. (of course at the node, x = 0, there is no transverse displacement of the pellet). If the displacement were equivalent to a 100-cm displacement of the wave then the pressure gradient deflections of Table II would be increased by a factor of 198 and the aerodynamic drag deflections would be 39 000 times larger. The maximum deflections at the quarter wave position (x = 600 cm) are 764 $\overline{\Delta x}_p$ and 584,000 $\overline{\Delta x}_u$ of Table III. By timing insertions within a small fraction of the period 0.012 s, the designer can select either of the displacements Δx_p or Δx_u or the vector sum (note that the time factor in Eq. (85) is squared) as desired. Thus even for a rapid repetition rate of 10/s, plus a modest exhaust orifice poorly designed, and for slow pellet insertion the 0.0099-cm maximum deflection at 0.5-cm asymmetry can be converted to a 0.00075-cm deflection for the same parameters, refer to Eqs. (83) and (85) , by slight changes in insertion time. At repetition rates lower than 10/s, the gas motion has died down and the chamber is simultaneously tolerant of large asymmetry, slow insertion, and low exhaust fraction leading to small damping.

VI. CONCLUSIONS

We find that for target circles of 1-mm diameter that pellet positional accuracies of about 0.3-mm are needed and that better accuracies are obtained in Antares CO_2 large laser designs.

With up to one atmosphere H_2 gas pressure and a 1-meter-long pneumatic gun, pellet velocities of the order of up to 10,000 cm/s are attainable with peak (initial accelerations) of 1000 g. The amount

TABLE III

MAXIMUM SUCCEEDING PELLET DISPLACEMENT, x, (0.5 cm ASYMMETRY)

Pulse	Wave Reflection Factor (ends)	Repetition Rate (s^{-1})	Pellet Insertion Velocity (cm/s)	Pressure Gradient Maximum Pellet Deflection at 0.5 cm from symmetry, x_p (cm)	Aerodynamic Drag Maximum Pellet Deflection at 0.5 cm from symmetry, x_μ (cm)
	0.84	1	13,770	3.0(-11)	4.5(-18)
	0.84	10	13,770	1.1(-5)	5.5(-7)
	0.84	1	449	2.8(-8)	6.2(-15)
	0.84	10	449	9.9(-3)	7.5(-4)
	0.5	1	13,770	1.3(-29)	7.9(-55)
	0.5	10	13,770	1.4(-7)	9.5(-11)
	0.5	1	449	1.2(-26)	1.1(-51)
	0.5	10	449	1.3(-4)	1.3(-7)

of H_2 released to the chamber at 1 atmosphere is less than $10^{12}/cm^3$, a negligible number at the upper densities considered here (10^{15} to $10^{17}/cm^3$). (Beam transport to and focusing on the pellet is likely to be a principal gas density and type limiting factor.) Residual chamber gas densities of $10^{17}/cm^3$ provide decelerations of 0.3 g or less (Ar and Li_2). Pellets typically can stand accelerations upward of 6000 g so structural damage is not expected from the processes considered here.

If the reaction chamber is kept at a vacuum, the residual gas densities and velocities from pellet debris at 5 mm asymmetry (of next pellet trajectory to previous pellet debris) have dropped to utterly negligible levels. Even using a monatomic i.e., a higher effect) and a repetition rate of 10/s the pellet trajectory deflection is less than 0.2 μm.

In the presence of a high density chamber gas (Ar at 10^{17} atoms/cm^3), small poorly designed exhaust orifices (100-cm radius square), high repetition rate (10/s), firing at peak ringing pressure, and with a slow insertion velocity (449 cm/s), one can achieve deflections of as much as 100 μm (Table III), but correction of any of these parameters leads to at least an order of magnitude improvement. Optimizing several leads to utterly negligible deflections.

In sum, neither the pellet structure, the available pellet accelerations, nor the highest expected chamber gas densities (nor the lowest) permitted by efficient laser beam transport, are any restraint upon pellet insertion save at high repetition rates (> 10/s) when the other parameters have latitude for, and require (at least some) optimization.

ACKNOWLEDGMENTS

It is a pleasure to acknowledge conversations and assistance from: J. Miller, W. Clouser, F. Harlow, H. Ruppel, R. Mills, H. G. Horak, E. Jones, G. Barasch, J. Zinn, R. Gentry, C. Mader, G. White, J. Munroe, T. Stratton, I. Bohachevsky, J. Goldstein, D. Dickman, and G. Fraley.

REFERENCES

1. J. J. Devaney, Los Alamos Scientific Laboratory, unpublished work (September 1977).
2. J. L. Munroe, Los Alamos Scientific Laboratory, unpublished work (September 1977).
3. R. C. Weast, ed., Handbook of Chemistry and Physics, 5th Ed., F52 (Cleveland, 1973).
4. D. E. Gray, ed., American Institute of Physics Handbook, 3rd ed., 2-262, 2-268 (McGraw-Hill, New York, 1972).
5. G. S. Fraley, Los Alamos Scientific Laboratory, personal communication (1977).
6. F. J. Dyson, "Free Expansion of a Gas, III," GAMD-566 (October 1958).
7. J. J. Devaney, Los Alamos Scientific Laboratory, unpublished work (July 7, 1977).
8. L. I. Sedov, Similarity and Dimensional Methods in Mechanics, M. Holt and M. Friedman, editors and translators (Academic Press, New York, 1959).
9. L. A. Booth, "Central Station Power Generation by Laser Driven Fusion," Los Alamos Scientific Laboratory report LA-4858-MS, V.I (February 1972).
10. F. H. Harlow and A. A. Amsden, "Fluid Dynamics," Los Alamos Scientific Laboratory report LA-4700 (1971).

APPENDIX

CORRECTION TO PNEUMATIC ACCELERATIONS FROM PELLET MOTION

In addition to viscosity and friction, a pellet accelerated down a tube by gas pressure suffers pressure loss from the rarefaction created by its own motion. We approximate the pressure reduction by that of a piston in a shock tube undergoing steady expansion with the same velocity. From Harlow and Amsden[10] the initial pressure P_0, density, ρ_0, and velocity of sound are related by

$$c_0 = \sqrt{\gamma P_0/\rho_0} = \sqrt{\gamma A_0 kT_0/M_A}\,, \qquad \text{(A-1)}$$

where γ is the ratio of specific heats; A_0 Avagadro's Number; kT_0 the initial temperature in energy units; and M_A, the molecular weight. The pressure, P, and sound velocity behind the pellet are

$$P = P_0(c/c_0)^{2\gamma/(\gamma - 1)}$$

$$P_0(c/c_0)\,, \qquad \text{(A-2)}$$

$$c = c_0 - \tfrac{1}{2}(\gamma - 1)v \equiv c_0(1 - bv), \qquad \text{(A-3)}$$

v is the velocity of the pellet. For convenience label

$$2\gamma/(\gamma - 1) \equiv \alpha\,, \qquad \text{(A-4)}$$

and

$$(\gamma - 1)/2c_0 \equiv b. \qquad \text{(A-5)}$$

Let the initial acceleration be

$$a_0 = AP_0/m, \qquad \text{(A-6)}$$

where A is the cross sectional area of the pellet and m its mass. Then from Eqs. (A-2), (A-3), and (A-6), the acceleration is given by

$$dv/dt = a_0(1 - bv)^{\alpha}, \qquad \text{(A-7)}$$

with solution for the initial conditions,

$$t = 0,\ v = 0, \qquad \text{(A-8)}$$

$$v = b^{-1}\left\{1 - \left[1 + a_0 b(\alpha - 1)t\right]^{-1/(\alpha - 1)}\right\} \qquad \text{(A-9)}$$

the distance travelled is

$$s = \int_0^t v\,dt = \frac{t}{b} + \frac{1}{a_0 b^2(\alpha - 2)}$$

$$\cdot\left\{1 - \left[1 + a_0 b(\alpha - 1)t\right]^{(\alpha - 2)/(\alpha - 1)}\right\}. \qquad \text{(A-10)}$$

Using (A-4) and (A-5) to replace α and b we get

$$v = \frac{2c_0}{\gamma - 1}\left\{1 - \left[1 + \frac{\gamma + 1}{2}\frac{a_0}{c_0}t\right]^{-(\gamma - 1)/(\gamma + 1)}\right\}, \qquad \text{(A-11)}$$

and

$$s = \frac{2c_0 t}{(\gamma - 1)} + \frac{2c_0^2}{a_0(\gamma - 1)}$$

$$\left\{1 - \left[1 + \frac{\gamma + 1}{2}\frac{a_0}{c_0}t\right]^{2/(\gamma + 1)}\right\}. \qquad \text{(A-12)}$$

$$v = 5c_0\left\{1 - \left[1 + 1.2\ a_0 t/c_0\right]^{-1/6}\right\}, \qquad \text{(A-13)}$$

$$s = 5c_0 t + (5c_0^2/a_0)$$

$$\left\{1 - \left[1 + 1.2\ a_0 t/c_0\right]^{5/6}\right\}. \qquad \text{(A-14)}$$

In the limit t or a_0/c_0 small (A-13) and (A-14) become

$$v = a_0 t, \qquad \text{(A-15)}$$

and

$$s = \tfrac{1}{2}\,a_0 t^2, \qquad \text{(A-16)}$$

whence

$$v = \sqrt{2a_0 s} \qquad \text{(A-17)}$$

as usual. For longer t or greater accelerations, t must be eliminated from (A-13) and (A-14) to obtain velocity as a function of distance.

Printed in the United States of America. Available from
National Technical Information Service
US Department of Commerce
5285 Port Royal Road
Springfield, VA 22161

Microfiche $3.00

001-025	4.00	126-150	7.25	251-275	10.75	376-400	13.00	501-525	15.25
026-050	4.50	151-175	8.00	276-300	11.00	401-425	13.25	526-550	15.50
051-075	5.25	176-200	9.00	301-325	11.75	426-450	14.00	551-575	16.25
076-100	6.00	201-225	9.25	326-350	12.00	451-475	14.50	576-600	16.50
101-125	6.50	226-250	9.50	351-375	12.50	476-500	15.00	601-up	

Note: Add $2.50 for each additional 100-page increment from 601 pages up.